Oxidation by DNA Charge Transport Damages Conserved Sequence Block II, a Regulatory Element in Mitochondrial DNA†

Edward J. Merino and Jacqueline K. Barton*

Division of Chemistry and Chemical Engineering, California Institute of Technology, Pasadena, California 91125

Received September 28, 2006; Revised Manuscript Received December 1, 2006

ABSTRACT: Sites of oxidative damage in mitochondrial DNA have been identified on the basis of DNA-mediated charge transport. Our goal is to understand which sites in mitochondrial DNA are prone to oxidation at long range and whether such oxidative damage correlates with cancerous transformation. Here we show that a primer extension reaction can be used to monitor directly oxidative damage to authentic mitochondrial DNA through photoreactions with a rhodium intercalator. The complex [Rh(phi)$_2$bpy]Cl$_3$ (phi = 9,10-phenanthrenequinone diimine) binds to DNA without sequence specificity and, upon photoactivation, either promotes strand breaks directly at the binding site or promotes one-electron oxidative damage; comparing the sites of base oxidation to direct strand breaks reveals the oxidative damage that arises from a distance through DNA-mediated charge transport. Significantly, base oxidation by charge transport overlaps with known mutational hot spots associated with cancers at nucleotides surrounding positions 263 and 303; the latter is known as conserved sequence block II and is vital to DNA replication. Since DNA base oxidation at conserved sequence block II should weaken the ability of damaged mitochondrial genomes to be replicated, DNA-mediated charge transport may provide a protection mechanism for excluding damaged DNA.

The mitochondrion contains an abundance of reactive oxygen species as a result of oxidative phosphorylation (*1*) and also plays a critical role in signaling apoptosis (*2*). Importantly, somatic and germ-line mutations in mitochondrial DNA (mtDNA)[1] have been detected in cells excised from a wide variety of tumors (*3*−*7*). MtDNA suffers from a mutation rate that is faster than that of nuclear DNA (*8*). Moreover, links between mitochondrial DNA mutations and cancer are thought to be associated with the biology of aging (*9*−*11*).

The molecular events leading to the formation of mtDNA mutations are in general poorly understood and can derive from a combination of factors. The nuclear-encoded mitochondrion replication and repair machinery, especially polymerase γ, can be impaired, leading to decreased fidelity (*12*). In tandem or alone, oxidative stresses caused by reactive oxygen species, small molecule carcinogens, and endogenous oxidants can lead to reactions centered at DNA nucleotides (*13*−*17*).

It is known that many mtDNA mutations prevalent in tumors have been localized within the control region of mtDNA (*18*, *19*). An area within the control region (Figure 1A, yellow) termed hypervariable II (Figure 1A, blue) contains regulatory elements, termed conserved sequence blocks (Figure 1A, red), that facilitate the cleavage and processing of a RNA transcript. The remaining short RNA transcript is used as a primer for DNA replication (*20*). Oxidative damage, and subsequent mutations, in hypervariable II may therefore have implications for mtDNA replication. This study aims to acquire a sequence level view of the oxidative damage pattern in hypervariable II of mtDNA.

Our laboratory has explored the chemistry of DNA-mediated charge transport and its biological consequences (*21*, *22*). We have shown that one-electron oxidative damage to DNA can arise from a distance as a result of hole migration through the DNA base pair stack (*23*, *24*). One-electron oxidation of DNA, in part, converts 2′-deoxyguanosine to 8-oxodeoxyguanosine and facilitates the misincorporation of an adenine instead of a cytosine during subsequent replication (*25*−*27*). Remarkably, oxidative DNA damage can occur at least 200 Å from the site of oxidant binding (*24*), and thus, its biological consequences require consideration. Long-range oxidative damage has been demonstrated both in nucleosomes (*28*, *29*) and within cell nuclei (*30*).

To identify sites of oxidative DNA damage that arise, we have taken advantage of the photochemistry of rhodium intercalators that contain the phenanthrenequinone diimine (phi) ligand (*31*). A phi intercalator bound to DNA sequence-specifically has been structurally characterized using X-ray crystallography (*32*). [Rh(phi)$_2$bpy]$^{3+}$ binds by intercalation to duplex DNA with low sequence specificity. Upon photoactivation at 313 nm, this complex promotes direct cleavage of the sugar phosphate backbone at the site of intercalation. With irradiation at lower energies, in contrast, the complex promotes base oxidation, yielding several oxidative products that can be revealed as strand breaks after the DNA is treated with piperidine (*23*). We first demonstrated oxidative damage

† We are grateful to the NIH (GM49216) for their financial support of this research, including a minority postdoctoral fellowship to E.J.M. We also thank the NFCR for their financial support.

* To whom correspondence should be addressed. E-mail: jkbarton@caltech.edu. Telephone: (626) 395-6075. Fax; (626) 577-4976.

[1] Abbreviations: phi, 9,10-phenanthrenequinone diimine; mtDNA, mitochondrial DNA; CSB, conserved sequence block.

10.1021/bi062024+ CCC: $37.00
Published on Web 02/16/2007

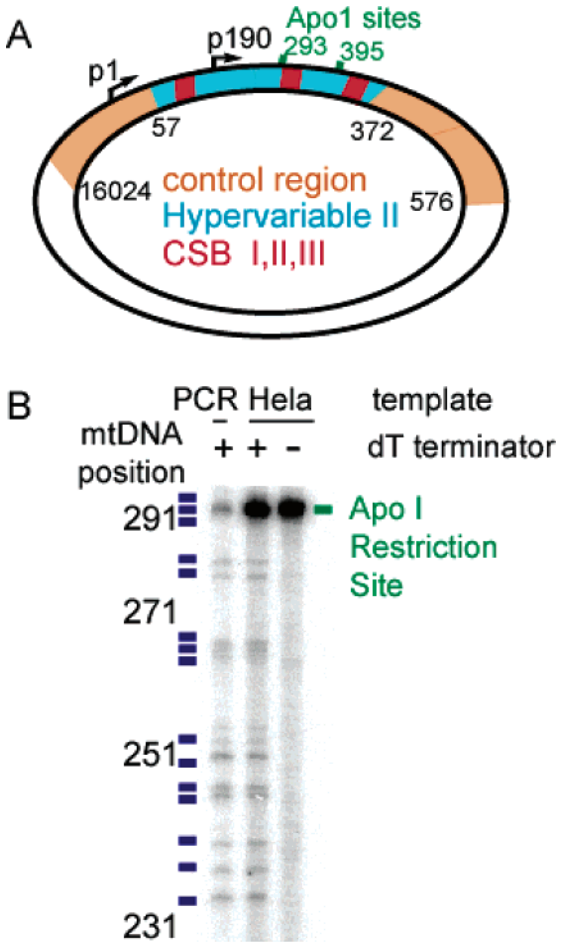

FIGURE 1: Accurate primer extension from total HeLa DNA. (A) The mitochondrial genome contains the noncoding control region (yellow, nucleotides 160−574). Regulation of DNA replication and transcription occurs in the hypervariable region (blue, nucleotides 57−372). The hypervariable region contains three conserved sequence blocks (red, nucleotides 213−235, 299−315, and 346−363) that are essential to DNA replication. Two primers (p1 and p190) are used to interrogate the oxidative damage pattern in hypervariable II. Restriction of both genomic and mitochondrial HeLa DNA with Apo I cleaves mitochondrial DNA at nucleotide 293 (green) within hypervariable II. (B) Primer extension of total HeLa DNA treated with Apo I yields a large band, indicating a single extension product. Addition of a dT terminator gives the termination products, as with manual sequencing, indicating extension occurs from the appropriate start site. The sequence is consistent with that of mitochondrial DNA.

from a distance (*23*) using phi complexes of rhodium tethered to the end of an oligonucleotide and spatially separated from guanine doublets in DNA; the 5′-guanines of guanine doublets and triplets are sites of particularly low oxidation potential (*33*). In a survey of larger regions of the genome, phi complexes cannot be tethered to the DNA and instead a noncovalent $[Rh(phi)_2bpy]^{3+}$ complex can be employed. By distinguishing simply between those strand breaks that result from higher-energy irradiation, marking rhodium binding sites, and lower-energy reaction, marking sites of one-electron oxidation, one can therefore identify damage to DNA that must arise from a distance.

To carry out these experiments in mtDNA with high sequence resolution, we developed a primer extension assay to visualize the oxidative damage in mtDNA. To date, ligation-mediated PCR has been more commonly employed in visualizing oxidative damage (*34*, *35*), but this assay contains several primer extension and amplification steps. Furthermore, because each cell has many mitochondria and each mitochondrion has several mtDNA genomes, mtDNA is approximately 10^3 times more abundant than nuclear DNA. Direct primer extension, then, without additional amplification, becomes an attractive alternative.

Here, we report the primer extension of mtDNA, in the presence of total HeLa DNA, after photolysis by $[Rh(phi)_2bpy]^{3+}$. We find that irradiation of the $[Rh(phi)_2bpy]^{3+}$−mtDNA complex yields strong oxidative damage within CSB II. Significantly, these sites of DNA damage overlap with mutations found in tumors.

MATERIALS AND METHODS

All experiments were carried out using fresh HeLa cells. HeLa cells (Sigma) were raised to ∼75% confluence, and total DNA was purified using the DNAeasy kit (Qiagen) and eluted from the column in 2.5 mM Tris (pH 8.5). Samples were then restricted and treated with RNAses (125 μL, 2 μg of HeLa DNA, 200 units of EcoRI, 0.25 mg of RNase, 25 °C, 20 min). Samples were purified using a PCR purification kit (Qiaquick, Qiagen), pooled, and stored at −20 °C (100 μL, 4 μg of total DNA, 5 mM phosphate, 25 mM NaCl, pH 7.4).

Base oxidation experiments were carried out using addition of 3 μM $[Rh(phi)_2bpy]Cl_3$. Samples were irradiated at 365 nm for 15 min by a 1000 W Hg/Xe lamp outfitted with a 320 long-pass filter, incubated with 99% piperidine (11 μL, 12 min, 95 °C) and cooled, and 9 μL of glacial acetic acid was added. The sample was prepared for primer extension by purification with a PCR purification kit (Qiaquick, Qiagen) to give 40 μL. The sample was divided into two 15 μL aliquots, and 15 μL of 2× reaction mix was added (2× taq buffer, 2 mM $MgCl_2$, 200 μM dNTP, 20 μM ^{32}P-end-labeled primer, and 0.3 unit/μL platinum taq). The sample was heated to 95 °C for 2.5 min and cycled 40 times for primer extension (55 °C for 40 s, 72 °C for 40 s, and 95 °C for 30 s). Samples were precipitated, and 6% denaturing PAGE was performed. Gels were visualized by overnight exposure to a phosphorimager screen and scanned. Direct strand scission was performed by irradiation at 313 nm on the 1000 W Hg/Xe lamp outfitted with a 295 long-pass filter, followed by purification without piperidine treatment and primer extension.

Primer p1 is 5′-ttaaataagacatcacgatgg, and p190 is 5′-gcacctacgttcaatattacaggcgaac. For manual sequencing, the control region was amplified by PCR by using appropriate primers. After purification, sequencing reactions were conducted by addition of acyclo-dNTP [1× Vent buffer, 100 μM dNTP, 66 μM acyclonucleotide, 3 μM ^{32}P-end-labeled primer, 10 units of Vent(exo$^-$)] and cycled as listed above. Data were quantified using the line function in ImageQuant (Amersham) and normalized in Excel.

RESULTS

Primer Extension Protocol. Direct primer extension can be optimized to visualize the sequence level information of oxidative lesions in mtDNA in a few hours. In this study, we used two primers, p1 and p190 (Figure 1), which are named for the mitochondrial position of the 3′-nucleotide. DNA is extracted from HeLa cells and treated with EcoRI

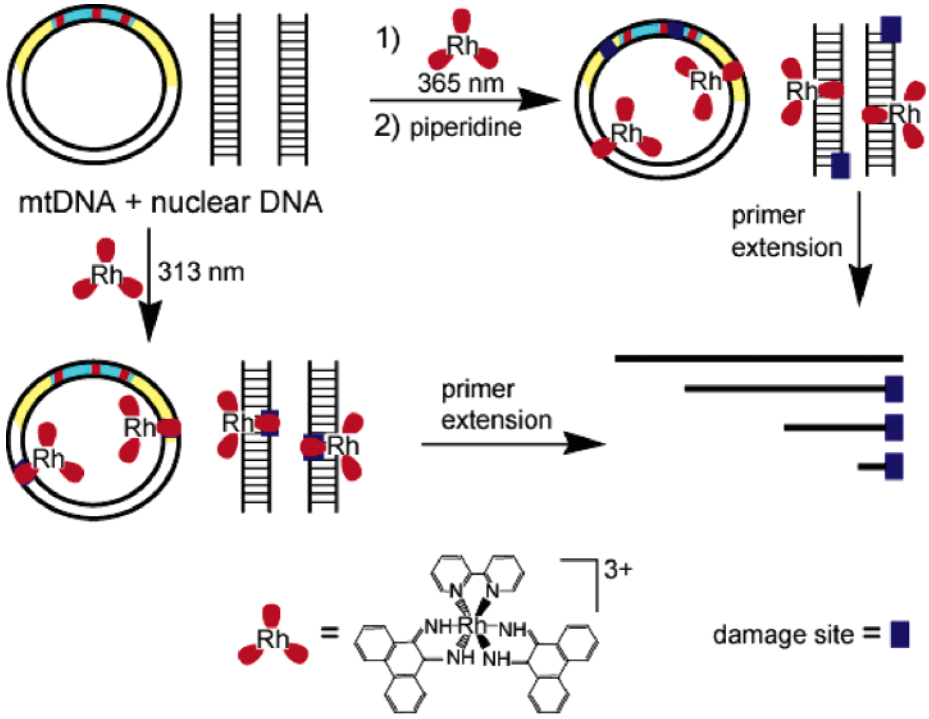

FIGURE 2: Schematic illustration of oxidative damage of total HeLa DNA with the Rh photooxidant. The $[Rh(phi)_2bpy]^{3+}$ intercalator (red) binds DNA without sequence selectivity. Irradiation of DNA-bound $[Rh(phi)_2bpy]^{3+}$ at 313 nm causes direct strand breaks at the site of intercalation (blue square). Instead, irradiation at 365 nm followed by piperidine treatment reveals sites of base oxidation with subsequent strand breaks that arise from DNA-mediated charge transport. Since the oxidative damage is generated from a distant photooxidant binding site, the site of base oxidation may differ from the intercalation site. Samples containing the strand breaks are then extended to reveal the oxidative damage pattern.

and RNase. EcoRI serves two purposes. (i) Restriction of DNA increases the efficiency of primer extension of mtDNA by removing supercoiling from the circular mitochondrial genome, and (ii) a decrease in the average nucleotide length allows a PCR purification kit to be used instead of ethanol precipitations. Each primer extension reaction mixture contains 4 μg of HeLa DNA extract, which corresponds to ~10 fmol of mtDNA.

Experiments were carried out to ensure correct and faithful primer extension of the HeLa DNA extract (Figure 1). Treatment of HeLa DNA with Apo I cleaves mitochondrial DNA at positions 293 and 395. Results are shown for extension with p190, which has a melting temperature of 60 °C and no secondary structure. After primer extension, a single band contains greater than 95% of the radioactivity and, compared to a manual sequencing lane, is located at mitochondrial position 293. Addition of dT terminator to the Apo I-treated HeLa DNA extract exactly matches manual sequencing.

Oxidative Damage with [Rh(phi)$_2$bpy]$^{3+}$. We then sought to determine the damage pattern of mtDNA photolyzed with $[Rh(phi)_2bpy]^{3+}$ at both high and low energies. Figure 2 shows our strategy for exploring long-range oxidative damage in mtDNA. Total Hela DNA extract, 1% mtDNA by weight, is incubated with $[Rh(phi)_2bpy]^{3+}$, to give one phi complex per 20 bp. Irradiation at 313 nm induces direct strand cleavage that cannot be extended by a polymerase. Therefore, the sequences bound and cleaved by $[Rh(phi)_2bpy]^{3+}$ can be directly interrogated. Lower-energy irradiation at 365 nm instead causes base oxidation. Addition of piperidine promotes backbone cleavage at the oxidized bases (*23*, *24*, *36*). After purification, a primer extension reaction is used to visualize the DNA damage pattern.

As an example, a portion of a gel using p190 is shown in Figure 3. Extension of p1 gives similar results. It should be noted that extension of HeLa DNA with p190 gives low background levels, and transcriptional stops at positions 298 and 312 (Figure 3, black squares) are observed. The transcriptional stops are consistent with known products of mtDNA replication in the growth phase (*37*−*39*). Addition of $[Rh(phi)_2bpy]^{3+}$ to the DNA sample without irradiation produces no change in the observed primer extension products {Figure 3, no $[Rh(phi)_2bpy]^{3+}$}. Incubation of the HeLa DNA extract with piperidine at 95 °C adds a small but measurable increase to the background {Figure 3; compare 313 nm to 365 nm without both light and $[Rh(phi)_2bpy]^{3+}$}. Irradiation of the DNA sample at low energy, 365 nm, without addition of $[Rh(phi)_2bpy]^{3+}$ but with piperidine treatment also causes little change in the extension products. Irradiation at high energy, 313 nm, with no $[Rh(phi)_2bpy]^{3+}$ causes a few additional specific termination products in the authentic HeLa DNA sample (Figure 3, empty boxes). Importantly, extension of mtDNA after it is photolyzed at either 313 or 365 nm in the presence of $[Rh(phi)_2bpy]^{3+}$ causes an observable damage pattern (Figure 3).

Figure 4 illustrates graphically, shown as a line plot of the gel lanes, another damage experiment with primer extension using p190. Irradiation with $[Rh(phi)_2bpy]^{3+}$ at 313 nm leads to direct strand breaks at all positions (Figure 4, red vs gray control). It should be recalled, however, that since cleavage here is assayed by extending the primer, shorter fragments will generally appear to have greater intensity (sites of lower nucleotide position). Nonetheless, while higher-molecular weight fragments are less intense and the cleavage pattern is not uniform across the region, all

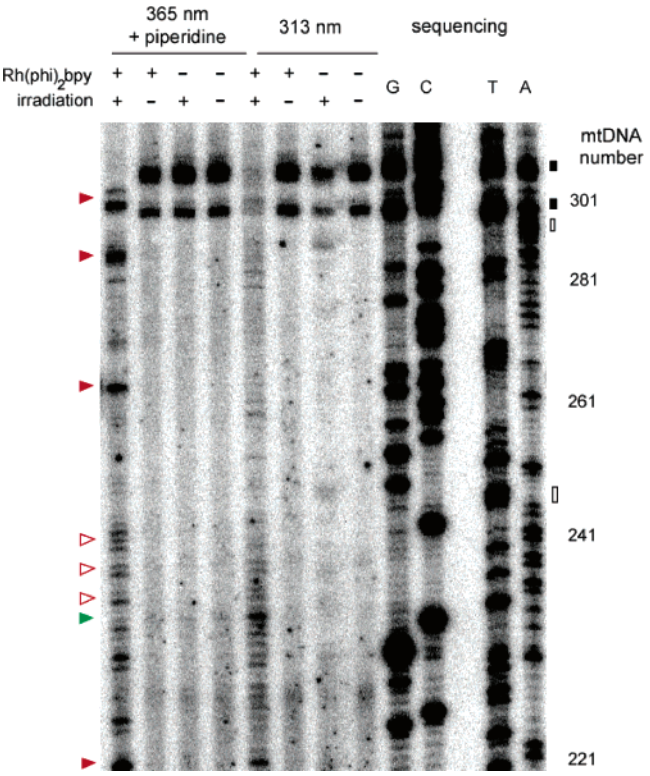

FIGURE 3: Representative gel showing DNA oxidation. Primer extension of total HeLa DNA shows a polymerase stop site at the top (black square). Control experiments where the oxidant, [Rh(phi)$_2$bpy]$^{3+}$, is omitted show low background. Irradiation at 313 nm without [Rh(phi)$_2$bpy]$^{3+}$ causes a small amount of photodamage (empty black square). Addition of [Rh(phi)$_2$bpy]$^{3+}$ and irradiation at 313 nm induces strand scission at the intercalation site (center of gel, green triangle). Addition of [Rh(phi)$_2$bpy]$^{3+}$ and 365 nm light followed by treatment with piperidine induces base oxidation with subsequent strand breaks (left portion of gel, filled red triangles for high damage, empty red triangles for moderate damage). Manual sequencing (right portion of gel) is used to relate the oxidative damage back to the mitochondrial DNA sequence (numbers). Note that the sites of base oxidation do not overlap with intercalation sites.

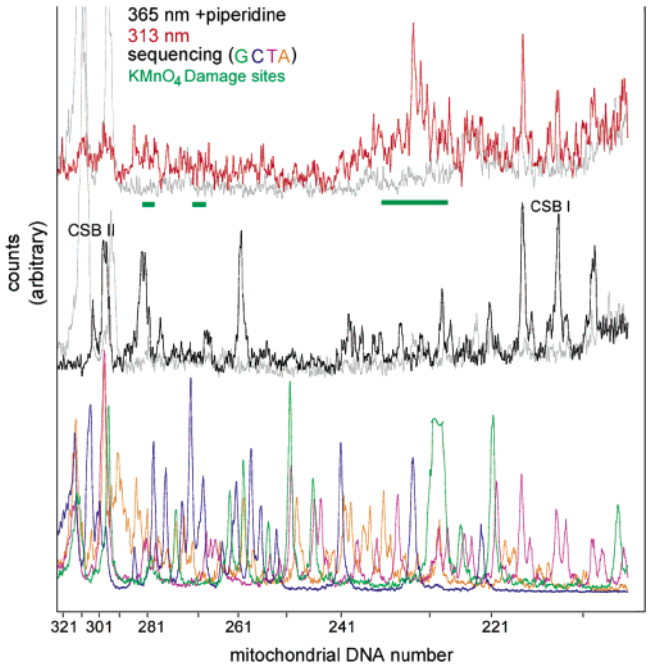

FIGURE 4: Phosphorimager line plot comparing the base oxidation pattern (black) and the sites of intercalation (red). Note there are few overlapping regions with large peak heights. Importantly, damage to conserved sequence block II occurs via charge transport from a distance.

fragments are represented, and few sharp bands are evident. Direct cleavage experiments show that binding by the Rh complex is not sequence-specific; as with other intercalators, some preference is found for 5′-pyrimidine-purine-3′ steps (*31*). Particularly strong cleavage by the Rh complex is found at position 218 as is oxidative damage, seen with irradiation at 365 nm and piperidine treatment. Also noteworthy is the hypersensitivity to [Rh(phi)$_2$bpy]$^{3+}$ photocleavage that is evident in the vicinity of position 230. Interestingly, reaction with $KMnO_4$ is also markedly enhanced in this region (see the Supporting Information); these observations are consistent with the greater chemical accessibility of this region of the genome.

Importantly, the damage patterns for [Rh(phi)$_2$bpy]$^{3+}$ followed by irradiation at 313 nm versus 365 nm with piperidine treatment (Figure 4; compare black and red plots) reveal key differences, reflecting sites preferentially bound by the Rh complex (313 nm) versus base sites strongly oxidized (365 nm). While photocleavage with [Rh(phi)$_2$bpy]$^{3+}$ at 313 nm reveals in general a low-intensity ladder pattern, strong damage is evident with 365 nm irradiation in the presence of the Rh complex and piperidine treatment at several sites distinct from those reflecting Rh binding (313 nm). As indicated above, irradiation at 313 nm shows two nucleotide regions, around 218 and 230 nm, as preferential binding sites based upon the increased peak height (Figure 4, highest peaks in the red line). With low-energy (365 nm) irradiation and piperidine treatment, positions surrounding position 230 show no base damage. Positions surrounding position 218 exhibit overlapping peaks (Figure 4, red and black lines). Therefore, position 230, with the strongest [Rh(phi)$_2$bpy]$^{3+}$ binding, is not the site where the most base oxidation occurs. Significantly, positions surrounding nucleotides 263, 290, and 303 do not exhibit high levels of preferential binding by [Rh(phi)$_2$bpy]$^{3+}$ but do exhibit strong damage after irradiation at 365 nm and piperidine treatment (Figure 4). Taken together, these data indicate that one-electron base oxidation by [Rh(phi)$_2$bpy]$^{3+}$ leads to DNA-mediated charge transport to regions of 263, 290, and 303 nm.

Line plots of p1 and p190 primer extension products of HeLa DNA treated with [Rh(phi)$_2$bpy]$^{3+}$ with and without irradiation at 365 nm are shown in Figure 5. Manual sequencing was used to map the sites of damage to the individual mtDNA position. Nucleotide positions 21−191 and 201−380 are visualized by p1 and p190 extension, respectively. Sites of damage were grouped into three sets: high, moderate, and little damage. Nucleotide positions where peak heights of the irradiated sample are 5 times greater than that of a sample lacking irradiation are termed high damage (Figure 5B, red). Likewise, samples with peak heights between 2.5 and 5 are termed moderate damage (Figure 5B, green).

Of the 360 mtDNA nucleotides in which Rh-monitored oxidative damage after photolysis at 365 nm is visualized, 43 nucleotides (12%) show moderate or high damage with an even distribution between the two types. Interestingly, 19 of the 22 positions with high damage are located within

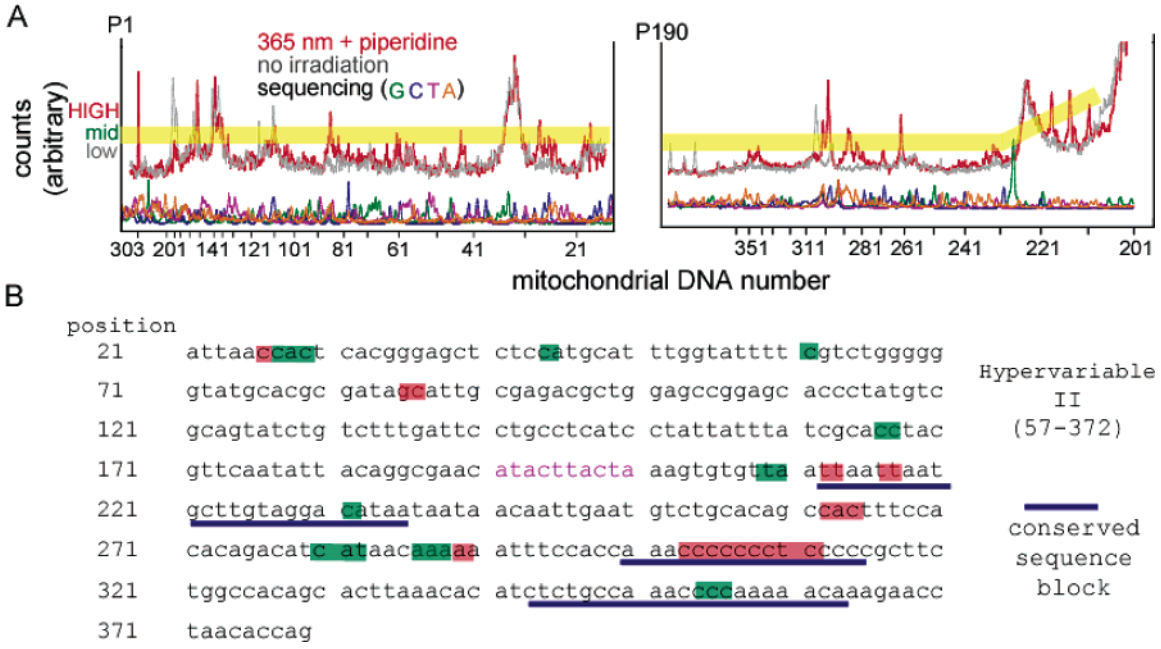

FIGURE 5: Sequences associated with DNA damage hot spots. (A) The damage pattern (red), obtained by a linear plot of the phosphorimaged gels, is compared to a sample not irradiated (gray). The mitochondrial DNA position is identified by comparison to manual sequencing ladders (bottom plot, various colors). Using two primers, p1 and p190, on a single sample indicates that the major areas of damage are at positions surrounding positions 86, 215, 290, and 263. (B) Superimposing the damage pattern on the sequence of mitochondrial DNA shows damage overlaps with conserved sequence block II.

the range of mtDNA positions 212−282. Therefore, 20% of the nucleotides visualized harbor 85% of the high-damage nucleotides, showing that this area is a hot spot for the localization of DNA damage.

Damage at guanosine and polyguanosine tracts is characteristic of a base oxidation by charge transport, since guanine doublets and triplets are the most easily oxidized sites in DNA (*33*). The heavy strand nucleotides that are damaged include 31 of 43 sequences with a guanine at or adjacent to the damage site (Figure 5B for a map of damage positions). At the nucleotide positions that are visualized, six of 17 polyguanosine tracts show interfering backgrounds. Of the remaining 11 polyguanosine tracts that could be visualized, seven fall into the moderate- or high-damage categories. Many of the remaining polyguanosine tracts show cleavage above background, but not sufficiently high to warrant labeling as moderate damage. Of note, the region with the highest damage level, near position 303, corresponds to the sequence 3′-G_7AG_5. Therefore, given the correlation between guanine tracts and damage, the oxidation potential does appear, as expected, to be a major determinant of oxidative damage. Areas of high damage are also located at nucleotides surrounding positions 86, 290, and 263. A few positions of high damage gave results not consistent with one-electron oxidation of DNA, however. The region near nucleotide 218 was shown to be a preferential $[Rh(phi)_2bpy]^{3+}$ binding site and $KMnO_4$ reaction site. Position 285 also exhibits high damage and contains the sequence T_5; reaction with $KMnO_4$ shows this site to be highly accessible to chemical modification (see the Supporting Information).

DISCUSSION

We have found that primer extension can be used to directly probe oxidative damage on authentic mtDNA in the presence of nuclear DNA. After addition of $[Rh(phi)_2bpy]^{3+}$ to total HeLa DNA followed by irradiation, preferential sites of binding $[Rh(phi)_2bpy]^{3+}$ can be visualized. Comparing the $[Rh(phi)_2bpy]^{3+}$ cleavage sites after irradiation at 313 nm to the oxidative damage sites induced by 365 nm irradiation followed by piperidine treatment reveals locations in the mtDNA genome that are preferentially damaged by charge transport from a distance. The sites tend to be polyguanosine tracts, known positions of low oxidation potential. Strong sites for oxidative damage at long range have been shown to arise independent of the oxidant employed as a damaging agent and thus reflect sites of particularly low oxidation potential, sites where electrons may be abstracted from a distance more easily (*21*, *24*). We infer from these data that, in general, these sites in mtDNA might represent regions to which oxidative damage is funneled.

Studies investigating the mutational frequency of germline mtDNA mutations in tumors (*18*, *19*) and other studies identifying frequencies associated with somatic mutations in cancer cells (*3*−*7*, *10*) have yielded strikingly similar results. Nucleotides located at positions 73, 263, and 303 are generally described as mutational hot spots. Significantly, our data, which define sites of one-electron oxidation by long-range charge transport, overlap with positions 263 and 303. We conclude, then, that mutations at positions 263 and 303 may likely be due to base oxidation by charge transport from an endogenous source, rather than reflective of the effects of impaired replication machinery. Indeed, sites of long-range base oxidation may provide a useful indicator of potential mutational hot spots.

From a biological perspective, the data also reveal a powerful correlation. We have found that the region that is most prone to oxidation by a charge transport mechanism coincides with CSB II. Conserved sequence block II holds a critical position in the mtDNA replication pathway (*38*).

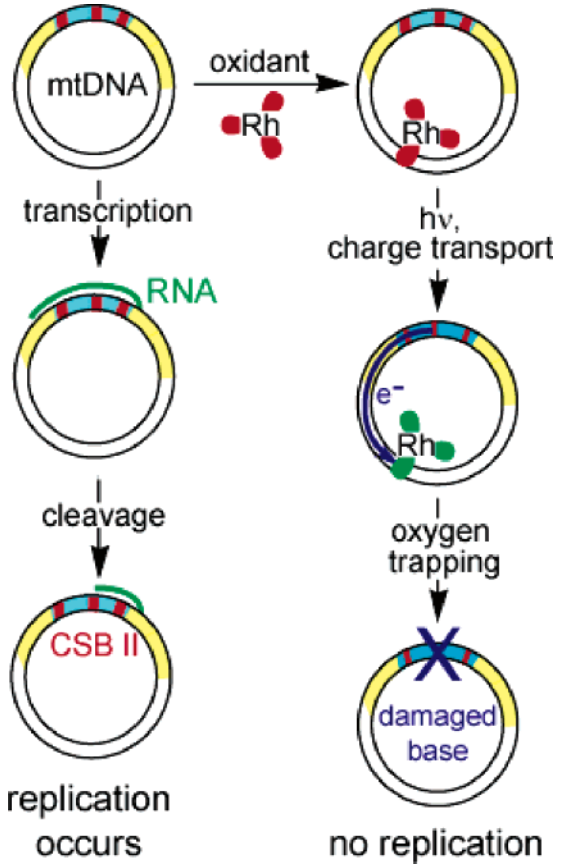

FIGURE 6: Oxidative damage by DNA-mediated charge transport, funneled to CSB II, provides a check point. Mitochondria replicate by a transcription-coupled mechanism. A RNA (green) is cleaved at the conserved sequence blocks (red) by a site-specific ribonuclease to form a RNA primer. The RNA primer is extended to make a new DNA strand. Since CSB II is a damage hot spot to which damage is funneled by charge transport (blue), localization of damaged bases could decrease the level of cleavage at CSB II. In this way, the replication mechanism amplifies undamaged DNAs. This site is also a mutational hot spot in tumor cells.

CSB II is recognized by a sequence-specific ribonuclease, RNAase MRP, that cleaves a RNA transcript to form a RNA primer for subsequent heavy strand synthesis in DNA replication (Figure 6). From these data, it is apparent that damage from one-electron oxidants is funneled to CSB II.

We hypothesize that damage at CSB II provides a valuable check point for DNA replication. Figure 6 shows schematically how this may work. Each cell contains many mitochondria that have numerous mtDNA genomes. Because of oxidative phosphorylation, a fraction of the mtDNA genomes will develop oxidative lesions. Oxidative lesions and subsequent mutations will be localized to CSB II. After transcription, unmodified mtDNA genomes will be recognized by RNase MRP and cleaved to form the synthesis primer at CSB II (Figure 6). The primer can then be used to make the new heavy strand. MtDNA genomes, with oxidative lesions or mutations, however, will not be recognized and cleaved at CSB II by the sequence-specific ribonuclease. Therefore, damaged mtDNA genomes will not be replicated. This mechanism serves to prevent damaged mtDNA from being propagated. Our hypothesis thus explains the sequence conservation in these blocks despite a highly mutable sequence. Finally, since many cancer and aging-associated mutations are present in CSB II, damaging the check point may eventually lead to disease.

In sum, these data illustrate a general method of exploring oxidative damage from a distance in large DNA regions and establish the specific sites in a regulatory region of mtDNA to which oxidative damage is funneled. Significantly, these regions map to CSB II, a known mutational hot spot found in tumors as well as a critical regulatory element for mtDNA replication. Localizing damage to this site may provide the cell with a protection mechanism by precluding the replication of damaged mtDNA.

SUPPORTING INFORMATION AVAILABLE

Phosphoimagery data for the reaction of mitochondrial DNA with $KMnO_4$ followed by primer extension. This material is available free of charge via the Internet at http://pubs.acs.org.

REFERENCES

1. Khrapka, K., Coller, H. A., Andre, P. C., Li, X. C., Hanekamp, J. S., and Thilly, W. G. (1997) Mitochondrial mutational spectra in human cells and tissue, *Proc. Natl. Acad. Sci. U.S.A. 94*, 13798−13803.
2. Kaufmann, S., and Earnshaw, W. C. (2000) Induction of apoptosis by cancer chemotherapy, *Exp. Cell Res. 256*, 42−49.
3. Fliss, M., Usadel, H., Caballero, O. L., Wu, L., Buta, M. R., Eleff, S. M., Jen, J., and Sidransky, D. (2000) Facile detection of mitochondrial DNA mutations in tumors and bodily fluids, *Science 287*, 2017−2019.
4. Parrella, P., Xiao, Y., Fliss, M., Sanchez-Cepedes, M., Mazzarelli, P., Rinaldi, M., Nicol, T., Gabreilson, E., Cuomo, C., Cohen, D., Pandit, S., Spencer, M., Rabitti, C., Fazio, V. M., and Sidransky, D. (2001) Detection of mitochondrial DNA mutations in primary breast cancer and fine-needle aspirates, *Cancer Res. 9*, 7623−7626.
5. Chen, J. Z., and Kadlubar, F. F. (2004) Mitochondrial mutagenesis and oxidative stress in human prostate cancer, *J. Environ. Sci. Health, Part C: Environ. Carcinog. Ecotoxicol. Rev. 22*, 1−12.
6. Polyak, K., Li, Y., Zhu, H., Lengauer, C., Willson, J. K. V., Markowitz, S. D., Trush, M. A., Kinzler, K. W., and Vogelstein, B. (1998) Somatic mutations of the mitochondrial genome in human colorectal tumours, *Nat. Genet. 20*, 291−293.
7. Tamura, G., Nishizuka, C., Maesawa, C., Suzuki, Y., Iwaya, T., Sakata, K., Endoh, Y., and Motoyama, T. (1999) Mutations in mitochondrial control region DNA in gastric tumours of Japanese patients, *Eur. J. Cancer 35*, 316−319.
8. Brown, W. M., George, M., and Wilson, A. C. (1979) Rapid evolution of animal mitochondrial DNA, *Proc. Natl. Acad. Sci. U.S.A. 76*, 1967−1971.
9. Wallace, D. C. (1992) Diseases of the mitochondrial DNA, *Annu. Rev. Biochem. 61*, 1175−1212.
10. Wang, Y., Michikawa, Y., Mallidis, C., Bai, Y., Woodhouse, L., Yarasheski, K. E., Miller, C. A., Askanas, V., Engel, W. K., Bhasin, S., and Attardi, G. (2001) Muscle-specific mutations accumulate with aging in critical human mtDNA control sites for replication, *Proc. Natl. Acad. Sci. U.S.A. 98*, 4022−4027.
11. Kang, D., and Hamasaki, N. (2005) Alterations of mitochondrial DNA in common diseases and diseased states: Aging, neurodegeneration, heart failure, diabetes, and cancer, *Curr. Med. Chem. 12*, 429−441.
12. Foury, F., Hu, J., and Vanderstraeten, S. (2004) Mitochondrial DNA mutators, *Cell. Mol. Life Sci. 61*, 2799−2811.
13. Harman, D. (1981) The aging process, *Proc. Natl. Acad. Sci. U.S.A. 78*, 7124−7128.
14. Croke, D. T., Blau, W., Ohuigin, C., Kelly, J. M., and McConnell, D. J. (1988) Photolysis of phosphodiester bonds in plasmid DNA by high-intensity UV laser, *J. Photochem. Photobiol., B 47*, 527−536.
15. Arkin, M. R., Stemp, E. D. A., Pulver, S. C., and Barton, J. K. (1997) Long-range oxidation of guanine by Ru(III) in duplex DNA, *Chem. Biol. 4*, 389−400.
16. Loft, S., and Poulsen, H. E. (1996) Cancer risk and oxidative DNA damage in man, *J. Mol. Med. 74*, 297−312.

17. Jackson, A. L., and Loeb, L. A. (2001) The contribution of endogenous sources of DNA damage to the multiple mutations in cancer, *Mutat. Res. 477*, 7−21.
18. Kurtz, A., Lueth, M., Kluwe, L., Zhang, T., Foster, R., Mautner, V. F., Hartmann, M., Tan, D. J., Martuza, R. L., Friedrich, R. E., Driever, P. H., and Wong, L. J. C. (2004) Somatic mitochondrial DNA mutations in neurofibromatosis type 1-associated tumors, *Mol. Cancer Res. 2*, 433−441.
19. Tan, D. J., Bai, R. K., and Wong, L. J. (2002) Comprehensive scanning of somatic mitochondrial DNA mutations in breast cancer, *Cancer Res. 62*, 972−976.
20. Shadel, G. S., and Clayton, D. A. (1997) Mitochondrial DNA maintenance in vertebrates, *Annu. Rev. Biochem. 66*, 409−435.
21. Delaney, S., and Barton, J. K. (2003) Long-range DNA charge transport, *J. Org. Chem. 68*, 6475−6483.
22. O'Neill, M. A., and Barton, J. K. (2004) DNA-mediated charge transport chemistry and biology, *Top Curr. Chem. 236*, 67−115.
23. Hall, D. B., Holmlin, R. E., and Barton, J. K. (1996) Oxidative DNA damage through long-range electron transfer, *Nature 382*, 731−735.
24. Nunez, M. E., Hall, D. B., and Barton, J. K. (1998) Long-range oxidative damage to DNA: Effects of distance and sequence, *Chem. Biol. 6*, 85−97.
25. Pinz, K. G., Shibutani, S., and Bogenhagen, D. F. (1995) Action of mitochondrial DNA polymerase γ at sites of base loss or oxidative damage, *J. Biol. Chem. 270*, 9202−9206.
26. Penta, J. S., Johnson, F. M., Wachsman, J. T., and Copeland, W. C. (2001) Mitochondrial DNA in human malignancy, *Mutat. Res. 488*, 119−133.
27. Hsu, G. W., Ober, M., Carell, T., and Beese, L. S. (2004) Error-prone replication of oxidatively damaged DNA by a high-fidelity DNA polymerase, *Nature*.
28. Nunez, M. E., Noyes, K. T., and Barton, J. K. (2002) Oxidative charge transport through DNA in nucleosome core particles, *Chem. Biol. 9*, 403−415.
29. Bjorklund, C. C., and Davis, W. B. (2006) Attenuation of DNA charge transport by compaction into a nucleosome core particle, *Nucleic Acids Res. 34*, 1836−1846.
30. Nunez, M. E., Holmquist, G. P., and Barton, J. K. (2001) Evidence for DNA charge transport in the nucleus, *Biochemistry 40*, 12465−12471.
31. Sitlani, A., Long, E. C., Pyle, A. M., and Barton, J. K. (1992) DNA photocleavage by phenanthrenequinone diimine complexes of rhodium(III): shape-selective recognition and reaction, *J. Am. Chem. Soc. 114*, 2303−2312.
32. Kielkopf, C. L., Erkkila, K. E., Hudson, B. P., Barton, J. K., and Rees, D. C. (2000) Structure of a photoactive rhodium complex intercalated into DNA, *Nat. Struct. Biol. 7*, 117−121.
33. Saito, I., Takayama, M., Sugiyama, H., and Nakatani, K. (1995) Photoinduced DNA cleavage via electron transfer: Demonstration that guanine residues located 5′ to guanine are the most electron-donating sites, *J. Am. Chem. Soc. 117*, 6406−6407.
34. Rodriguez, H., Akman, S. A., Holmquist, G. P., Willson, G. L., Driggers, W. J., and LeDoux, S. P. (2000) Mapping oxidative DNA damage using ligation mediated polymerase chain reaction technology, *Methods 22*, 148−156.
35. Driggers, W. J., Holmquist, G. P., LeDoux, S. P., and Willson, G. L. (1997) Mapping frequencies of endogenous oxidative damage and the kinetic response to oxidative stress in a region of rat mtDNA, *Nucleic Acids Res. 25*, 4362−4369.
36. Burrows, C. J., and Muller, J. G. (1998) Oxidative nucleobase modifications leading to strand scission, *Chem. Rev. 98*, 1109−1151.
37. Fish, J., Raule, N., and Attardi, G. (2004) Discovery of a major d-loop replication origin reveals two modes of human mtDNA synthesis, *Proc. Natl. Acad. Sci. U.S.A. 306*, 2098−2101.
38. Clayton, D. A. (1991) Replication and transcription of vertebrate mitochondrial DNA, *Annu. Rev. Cell Biol. 7*, 453−478.
39. Xu, B., and Clayton, D. A. (1996) RNA-DNA hybrid formation at the human mitochondrial heavy-strand origin ceases at replication start sites: An implication for RNA-DNA hybrids serving as primers, *EMBO J. 15*, 3135−3143.

BI062024+